Food Hydrocolloids 57 (2016) 280–290

Contents lists available at ScienceDirect

Food Hydrocolloids

journal homepage: www.elsevier.com/locate/foodhyd

Spontaneous co-assembly of lactoferrin and β-lactoglobulin as a promising biocarrier for vitamin B9

Anne-Laure Chapeau [a, b, d], Guilherme M. Tavares [a, b, c], Pascaline Hamon [a, b], Thomas Croguennec [a, b], Denis Poncelet [d], Saïd Bouhallab [a, b, *]

[a] INRA, UMR 1253 Science and Technology of Milk and Egg, 35042 Rennes, France
[b] Agrocampus Ouest, UMR 1253 Science and Technology of Milk and Egg, 35042 Rennes, France
[c] Laboratory Research in Milk Products, 36570 Vicosa, Brazil
[d] ONIRIS, UMR CNRS GEPEA 6144, 44322 Nantes, France

ARTICLE INFO

Article history:
Received 5 November 2015
Received in revised form
26 January 2016
Accepted 3 February 2016
Available online 10 February 2016

Keywords:
Whey proteins
Heteroprotein co-assembly
Complex coacervation
Bioactive
Vitamin
Biocarrier

ABSTRACT

The design of biocarriers for protection and controlled delivery of bioactives represents a challenge for developing functional foods. We investigated the potentiality of heteroprotein Beta-lactoglobulin (BLG) and Lactoferrin (LF) co-assemblies as biocarriers for vitamin B9 (B9). Using different B9:protein mixing ratios, B9-LF-BLG co-assemblies were obtained and assessed by turbidity and phase contrast microscopy. Kinetics of their formation and stability were monitored. B9 entrapment efficiency was evaluated. Two types of B9-LF-BLG co-assembly were identified: aggregates (at low and high protein concentrations), and heteroprotein coacervates (at intermediate protein concentrations), both exhibiting different kinetics and stability over time. Compiling screening maps of B9-LF-BLG co-assemblies and B9 entrapments, we evidenced that B9-LF-BLG coacervates exhibited higher performance as B9 biocarrier, with an optimal entrapment of ≈10 mg B9/g protein. Therefore, such co-assembly displays useful potentialities as vitamin biocarriers for the design of natural functional foods, offering enhanced health benefits, yet without resorting to non-food additives.

1. Introduction

Our food diet is often described as our first medicine. In recent years, there has been a growing demand from consumers for food products offering health benefits (Annunziata & Vecchio, 2011; Biesalski et al., 2009). To meet this demand, the food industry has sought to enhance the nutritional qualities of traditional food products by enriching them with bioactive compounds such as polyphenols, fatty acids or vitamins. It has led to the creation of a whole range of new functional food products (Betoret, Betoret, Vidal, & Fito, 2011). However, the design of these products requires to overcome two main technological challenges. Firstly, the bioactive compounds may be poorly soluble into the desired food product, thereby limiting the feasibility of product enrichment (Diarrassouba, Garrait, et al., 2015). Secondly, the bioactive compounds are often very sensitive to the conditions applied during food processing and storage, thereby limiting their actual bioavailability as intact constituents of the functional food products (Hosseini, Emam-Djomeh, Sabatino, & Van der Meeren, 2015). A way to overcome these two main issues and to ensure the effective delivery of the bioactive compounds is to load, protect and release the bioactives by means of structures called biocarriers (Shimoni, 2009). As a result, the design of these biocarriers appeared as a key challenge to develop functional food products (Chen, Remondetto, & Subirade, 2006; Lacatusu et al., 2013). In addition to their demand for functional food products, consumers tend also to favor food products with minimal amount of additives. As a result, it could be relevant to use directly some components of the targeted food product as biocarrier materials for the bioactives. This approach has the potential to ensure the design of functional and natural foods, enabling additive-free food products, well-known in the food industry sector as “clean label” or “green product” (Diaz, 2013). Following this approach, we address here the exploitation of milk components to create biocarriers for bioactives in order to design functional and natural dairy products, offering enhanced health benefits.

* Corresponding author. INRA, UMR 1253 Science and Technology of Milk and Egg, 35042 Rennes, France.
E-mail address: said.bouhallab@rennes.inra.fr (S. Bouhallab).

http://dx.doi.org/10.1016/j.foodhyd.2016.02.003
0268-005X/

Among food components, food proteins are biopolymers that appear suitable for the protection of several bioactives due to their capacity to establish various types of interactions with other compounds (Diarrassouba, Remondetto, et al., 2015). In addition, food proteins are generally recognized as safe (GRAS), which make them interesting biopolymers for the conception of biocarriers (Chen et al., 2006). In this regard, milk proteins have been specifically studied for the design of biocarrier systems, due to their versatility and excellent functional properties (Tavares, Croguennec, Carvalho, & Bouhallab, 2014). Many strategies were developed to use milk proteins as biocarriers such as formation of simple complexes with ligands, formation of gel networks by means of covalent, hydrophobic or hydrogen interactions, and formation of supra-molecular structures through electrostatic interactions (Bouhallab & Croguennec, 2014; Diarrassouba, Remondetto, et al., 2015; Schmitt, Aberkane, & Sanchez, 2009). Among milk proteins, Beta-lactoglobulin (BLG) and Lactoferrin (LF) exhibit various characteristics that make them good candidates for the design of biocarriers for bioactive compounds. BLG is a globular acidic protein (pI = 5.2) and constitutes the major whey proteins. BLG has been identified to bind various ligands either hydrophobic such as curcumin, vitamin E (Eratte, Wang, Dowling, Barrow, & Adhikari, 2014; Liang, Tremblay-Hébert, & Subirade, 2011; Teng, Li, & Wang, 2014), fatty acids, or hydrophilic such as vitamin B9 (Pérez-Masiá et al., 2015; Zhang, Liu, Subirade, Zhou, & Liang, 2014). Lactoferrin (LF) is an iron-binding glycoprotein folded into two symmetrical lobes (the N-lobe and C-lobe). LF is a basic protein (pI = 8.6) and thus carries positive electric charges at neutral and acidic pH. LF is a multifunctional protein with immunomodulatory, antimicrobial and antioxidant properties. Furthermore, recent studies have reported the ability of BLG and LF to spontaneously co-assemble to form two types of supra-molecular structures: aggregates or heteroprotein complexes called “coacervates” through a process of complex coacervation (Anema & (Kees) de Kruif, 2014; Tavares, Croguennec, Hamon, Carvalho, & Bouhallab, 2015). The shape of co-assembly depends strongly on the total protein concentration and protein stoichiometry of the system (Anema & (Kees) de Kruif, 2014; Bouhallab & Croguennec, 2014; Yan et al., 2013). Heteroprotein aggregation is often described as a kinetically controlled process. The resultant aggregates are typically fractal objects, which form often irreversible supra-molecular structures (Bouhallab & Croguennec, 2014; Yan et al., 2013). Complex coacervation is a spontaneous co-assembly occurring between two oppositely charged biopolymers and leading to phase separation (Bungenberg de Jong, 1949; Overbeek & Voorn, 1957). It generates the formation of two separated liquid phases: the dilute phase, rich in solvent and poor in biopolymers and the dense phase, concentrated in biopolymers, namely, complex coacervates (Schmitt et al., 2009). Complex coacervates are often reported as microspheres due to their μm size dimension and their spherical shapes. Moreover, they are often suggested as interesting biocarriers for biocative compounds (de Vos, Faas, Spasojevic, & Sikkema, 2010; Ezhilarasi, Karthik, Chhanwal, & Anandharamakrishnan, 2013; Gouin, 2004; Tavares et al., 2014). Complex coacervation has been mostly studied for proteins/polysaccharides systems (de Kruif, Weinbreck, & de Vries, 2004; Schmitt & Turgeon, 2011) and its potential applications for encapsulation as well (McClements, 2015; Ron, Zimet, Bargarum, & Livney, 2010; Schmitt, Sanchez, Desobry-Banon, & Hardy, 1998). Nevertheless, few studies have been done to determine whether heteroprotein complex coacervation can be used for encapsulation. In this regard, complex coacervation between BLG and LF appears as good candidate as biocarrier for bioactives.

Among bioactive compounds, the vitamin B family is of great interest owing to its vital importance and biological role (Lucock, 2000). Folic acid, currently known as vitamin B9, is involved in several biochemical processes: DNA synthesis and repair, cell division and co-enzyme in carbon metabolism pathways, including the biosynthesis of several amino acids (Araújo et al., 2015). B9 has been recognized to provide several health benefits such as preventing cardiovascular diseases (Adank, Green, Skeaff, & Briars, 2003), colon cancer (Sanjoaquin, Allen, Couto, Roddam, & Key, 2005), or congenital malformations during pregnancy (Lucock, 2000; Moat et al., 2004). Nevertheless, humans cannot synthesize B9 and therefore must find sufficient sources of B9 in their daily diet (Basset, Quinlivan, Gregory, & Hanson, 2005). B9 deficiency is relatively common among the vulnerable populations such as elderly people or pregnant women (Mills & Signore, 2004). As a result, there is a need for developing foods and drinks enriched in B9 (Gregory, 2001). However, this appears as a technological challenge due to the poor solubility of B9 at acidic pH. Hence, to successfully enrich acidic food products with B9, the design of specific biocarriers for this vitamin is required. Furthermore, in literature, numerous studies and reviews can be found on the design of biocarriers for lipophilic bioactive compounds such as fatty acids, polyphenols, flavor compounds or oil-soluble vitamins (Champagne & Fustier, 2007; de Vos et al., 2010; Fang & Bhandari, 2010; Matalanis, Jones, & McClements, 2011; McClements, Decker, & Park, 2009; Xiao, Liu, Zhu, Zhou, & Niu, 2014). Nevertheless, the design of biocarriers for hydrophilic bioactive compounds such as B9 has been the subject of little attention and stays rather specific (He et al., 2015; Liang, Leung Sok Line, Remondetto, & Subirade, 2010; Pérez-Masiá et al., 2015). Here we examine in details the potentiality of the spontaneous co-assembly between LF and BLG at pH 5.5 as biocarriers for the hydrophilic vitamin B9, given that B9 interacts with LF (Tavares, Croguennec, Lê, et al., 2015). In this previous work, we showed that LF can bind until 10 mol of FA throughout electrostatic interactions following a two-step mechanism: interaction and subsequent self-association of the complexes. Here, co-assembly between LF and BLG in the presence of B9 was investigated across a range of physico-chemical conditions and the co-assembly yields were evaluated. The formation kinetics of B9-LF-BLG co-assemblies were monitored. The final morphology and the biocarrier efficiency of formed B9-LF-BLG co-assemblies were determined.

2. Materials and methods

2.1. Stock solutions

Lactoferrin (LF) from bovine milk, purity 90% and iron saturation level of 10%–20% according to the manufacturer's specifications, was purchased from the Fonterra Cooperative Group, New Zealand. LF powder was used without modification. Beta-Lactoglobulin (BLG) powder was obtained from a confidential industrial source. Its composition (w/w) was: protein 93.5%, moisture 4% and ash <1.8%. Protein purity was determined by reversed-phase HPLC and no proteins other than BLG were detected. BLG powder was dispersed in deionized water (45 g/L), adjusted to pH 4.6 with 1 M HCl and kept at 30 °C for 5 min in order to precipitate non-native forms of BLG. The dispersion was centrifuged at 20,000 g at room temperature for 10 min (Heraeus Biofuge Primo, Thermo Scientific, Waltham, MA, USA). BLG suspension was then freeze-dried and stored at −20 °C until use.

LF and BLG stock solutions were prepared by solubilizing the protein powders in milli-Q water and their pH were adjusted at pH 5.5 using 1 M HCl solution. The protein solutions were filtered through a 0.45 μm and a 0.2 μm membrane (cat. no. 4612, Pall Corporation, Ann Arbor, MI, USA). The exact proteins concentrations were determined by absorbance at 280 nm (spectrometer

UVmc^2, Safas, Monaco) using 1.47 L g^{-1} cm^{-1} and 0.96 L g^{-1} cm^{-1} as extinction coefficients for LF and BLG respectively. The stock solutions were prepared to have a concentration of LF = 0.5 mM (41.5 g L^{-1}) and BLG = 1 mM (18.3 g L^{-1}).

Vitamin B9 (B9) was purchased from Sigma–Aldrich (Folic acid, purity ≥ 97%, Sigma Aldrich, St. Louis, MO, USA). B9 stock solution was prepared by solubilizing the vitamin powder in milli-Q water and then adjusted to pH = 5.5 using 1 M HCl solution. B9 solution was centrifuged at 28,000 g for 30 min at room temperature (centrifuge Hereaus Biofuge primo, KENDRO Laboratory products, Courtabœuf, France). The supernatant was filtered through a 0.2 μm membrane (cat. no. 4612, Pall Corporation, Ann Arbor, MI, USA). The exact vitamin B9 concentration was determined by absorbance at 283 nm (spectrometer UVmc^2, Safas, Monaco) using 25,100 M^{-1} cm^{-1} as extinction coefficient.

LF, BLG and B9 stock solutions were stored at 4 °C and protected from UV light radiation.

2.2. Experimental solutions

A series of solutions of B9-LF-BLG were prepared following a range of B9:protein mixing ratios, where Protein refers to LF + BLG total content. To obtain the required concentrations of B9, LF, and BLG according to each ratio, the stock solutions were diluted into the proper volume of milli-Q water at pH = 5.5. The tested concentration ranges of diluted stock solutions were 0–0.5 mM for B9 and 0–1.1 mM for proteins (LF + BLG). Then for each ratio, the three corresponding diluted solutions were mixed together, following the same procedure. LF and B9 were first mixed together and let to homogenize for 10 min, then BLG was added to the system. We studied a range of B9:total protein ratios from 1:1 to 10:20. Low numerical values refer to lowest concentrations of components studied while high values refer to the highest concentrations tested. In this study, BLG/LF molar ratio of 10, reported to be optimum for coacervation (Tavares, Croguennec, Hamon, et al., 2015) was kept constant. All B9-LF-BLG mixed solutions were prepared at room temperature (20 °C ± 2 °C), and no significant modification of pH was detected after mixing.

2.3. Zeta potential and hydrodynamic diameter measurements

The zeta potential of experimental solutions was measured using a Zetasizer NanoZS (Malvern Instruments, Malvern, U.K.). 700 μL of solution were put into a folded capillary cell (DTS1061, Malvern, U.K.), and after 2 min of equilibration an electric potential of 150 V was applied. The dielectric constant and the refractive index of the solvent were set at 78.5 and 1.333, respectively. The electrophoretic mobility was calculated applying the Henry equation, and the zeta potential was calculated using the Smoluchowski approximation. The measured zeta potential values were: LF: +7.2 mV, BLG: −8.4 mV, FA: −0.035 mV. The zeta potential of a mix containing FA/(LF + BLG) at molar proportions of 5/(1 + 10) was −1.9 mV.

The hydrodynamic diameters (Dh) of different B9-LF-BLG complexes were determined by dynamic light scattering (DLS) using a Zetasizer NanoZS (Malvern Instruments, Malvern, U.K.). Dh was calculated using the Stokes–Einstein equation, assuming that the complexes were of spherical shape. The dynamic light backscattering was detected at 173°, and a refractive index of 1.45 for the complexes was used for volume-size representation. Dh measurements were performed at 25 °C, after an equilibration time of 2 min. The results were the means of at least 13 runs, and all samples were analyzed in triplicate.

2.4. Turbidity measurements

Turbidity measurements were performed at 600 nm (A_{600nm}) with the spectrometer UVmc^2 (Safas, Monaco) to monitor the co-assembly in B9-LF-BLG solutions. Absorbance measurements were converted to turbidity (τ, cm^{-1}) using the following relationship: $\tau = (2.303A_{600nm})/l$, where l is the light path length ($l = 1$ cm). Turbidity was monitored over 180 min. Under the ratios investigated, the LF, BLG and vitamin B9 stock solutions alone had no detectable turbidity.

2.5. Phase contrast microscopy and co-assembly type index

The presence of aggregates, coacervates, or the absence of supra-molecular structures was determined using a phase contrast optical microscope (Olympus BX51TF, Olympus, Hamburg, Germany) set at the magnification × 40. A 10 μL sample of the B9-LF-BLG solutions was taken at the time of maximum turbidity and immediately observed. Time of maximum turbidity was defined as the time after which no further rise of turbidity was detected after 150 min. In order to code the type of supra-molecular structures observed for each B9-LF-BLG solution a notation scale was set up. The scale, called “co-assembly type index”, was as followed: 0: no observable microparticles co-assembly, 1: aggregates, 2: few and dispersed coacervates, 3: rather dense coacervates, 4: very dense and numerous coacervates. As we focused on microscopic structures, the formation of nanoparticles and nano-complexes under some mixing conditions is not excluded. The samples and observations were performed three times on each solution to ensure the representability of the results.

2.6. Solution stability

The stability of the B9-LF-BLG co-assemblies was monitored using the optical characterization method with a TurbiScan (Turbiscan Laboratory Formulation, Ramonville St. Agne, France). The analyzed solution is placed in a cylindrical glass cell of 4 mL (diameter = 12 mm, height = 25 mm). The light source is an electro luminescent diode emitting at λ = 850 nm. The light source scans the solution at 1 min intervals from top to bottom. Two synchronous optical sensors receive respectively the light transmitted through the solution (180° from the incident light, transmission sensor), and the light backscattered by the solution (45° from the incident radiation, backscattering detector). Each scan provides the profiles of the transmitted and backscattered light flux (%) relative to standards (suspension of monodisperse spheres and silicone oil) as a function of the solution height (mm). These two curves could be considered to be macroscopic “fingerprint” of each solution at a given time (Kowalska, Zbikowska, & Tarnowska, 2015). Moreover the backscattering signal is directly related to the photon transport mean free path. Thus Backscattering intensity depends on particle size and concentration. The mixing of B9-LF-BLG was realized directly in the cylindrical glass cell of measurements according to the B9:protein ratio tested. For each sample, the TurbiScan analysis was carried out for 24 h, at 20 °C.

2.7. Co-assembly yield and entrapment efficiency

B9 and protein contents were quantified in order to determine their recovery yield in the co-assemblies. For each B9-LF-BLG solution, the supernatant and the dense phase of co-assembly were separated by centrifugation (Heraeus Biofuge Primo, Thermo Scientific, Waltham, MA, USA) at 28,000 g for 30 min. B9 and proteins recovered in the supernatant were quantified after separation by reversed-phase high-performance liquid chromatography (RP-

HPLC), using a LiChrospher RP-18 column (Merck, Darmstadt, Germany) connected to a Waters 2695 HPLC system. B9 and total proteins were eluted at a flow rate of 0.4 mL min^{-1} using an isocratic gradient of Acetonitrile/milli-Q water 40/60 (v/v) containing 100 μL L^{-1} of 1 M NaOH and quantified by absorbance at 283 nm. The quantities of B9 and proteins in the co-assemblies were calculated by subtracting the quantities in the supernatant from the initial quantities.

The quantities of B9 and proteins recovered in the co-assemblies were used to calculate four key parameters for each B9-LF-BLG solution according to the following equations:

the co-assembly yield η,

$$\eta = \frac{[Protein + B9]_{co-assembly}}{[Protein + B9]_{total}}$$

the B9 loading,

$$B9\ Loading = \frac{[B9]_{co-assembly}}{[Protein + B9]_{co-assembly}}$$

the entrapment of B9 within the co-assembly (mg B9/g protein),

$$Entrapment = \frac{Q_{B9\ co-assembly}}{Q_{Protein\ co-assembly}}$$

and the entrapment efficiency of B9 (%),

$$Entrapment\ efficiency = \frac{Q_{B9\ co-assembly}}{Q_{B9\ initial\ solution}}$$

with [protein] and [B9] the concentration in mM in the initial solution or recovered in the co-assembly, and Q the quantity of B9 (mg) and protein (g) in the co-assembly or in the initial solution. Chromatographic quantifications were performed to check that no significant degradation of B9 occurred during our experiments and analyses.

2.8. Screening maps of B9-LF-BLG co-assembly

Screening maps are a color projection of a specific parameter (maximum turbidity in cm^{-1}, co-assembly type index, or entrapment in mg B9/g protein) as a function of the B9:protein mixing ratios. Each screening map plots the specific value of one parameter obtained from a specific B9:protein ratio. Screening maps were plotted using the OriginPro 2015 software. The Renka-cline gridding method was used to convert the random XYZ data to matrices. Then the screening maps were plotted using the XYZ contour graph method of the software.

2.9. Particle size and sphericity analysis

Particle size and sphericity analysis were measured by dynamic image analysis using a Qicpic™ analyzer (Sympatec GmbH, Clausthal-Zellerfeld, Germany). Measures were performed using the SUCELL wet dispersion unit. Data were analysed using WINDOX 5 software (Sympatec LTD, Bury, UK). The principle and the validity of the measurements by this method had been detailed previously by (Hamilton, Littlejohn, Nordon, Sefcik, & Slavin, 2012). Briefly, fast camera records digital images of the particles dispersed in solution. Proprietary algorithm of the software WINDOX 5 are then used to analyze each images and lead here to the calculation of the two parameters: the equivalent projected circle (EQPC) diameter, which gives the diameter of a sphere that has the same 2-dimensional area as the projected particle in the recorded image, reported as the particle size (in μm) in this study, and the sphericity which is the ratio of the perimeter of the equivalent circle P_{EQPC} to the real perimeter of the particle P_{real}. This value is between 0 and 1. The smaller the value, the more irregular the particle shape is. For measurement, a volume of 5 mL of the B9-LF-BLG solution was dispersed into the cell of the wet dispersion unit containing 50 mL of milli-Q water. The detection was set to 1% and the recorded film lasted 60 s. Analysis were performed three times for each solution.

3. Results and discussion

3.1. LF-BLG co-assemblies in the presence of B9

Recently, we reported on the ability of BLG and LF to co-assemble at pH 5.5 into either coacervates or aggregates according to initial total protein concentrations (Tavares, Croguennec, Hamon, et al., 2015). We also showed and discussed the inhibition of BLG and LF co-assembly at extreme concentrations. To assess that BLG and LF can also co-assemble in the presence of B9, six B9:protein ratios were tested: two ratios at low protein contents (2:2 and 4:2), two ratios at intermediate protein contents (2:11 and 4:11), one ratio at high protein content (4:15) and one ratio at very high protein content (4:20). The protein concentration range was chosen to form either coacervates or aggregates according to the previous results obtained without B9 (Tavares, Croguennec, Hamon, et al., 2015).

Fig. 1 shows the turbidity kinetics obtained with the six solutions tested. Turbidity increased for all the ratios as soon as BLG was added into the B9+LF solutions, except for the solution with the highest protein content (4:20). These increased turbidities reflected the co-assembly into supramolecular structures, defined as microparticles, taking place in the B9-LF-BLG solutions. To correlate these turbidity profiles with the formation of microparticles, a study by phase contrast microscopy was conducted. Fig. 2 shows the microscopic images obtained by the phase contrast microscopy analysis performed on the six solutions, at maximum turbidity. Two types of turbidity profiles and microparticles can be identified. The

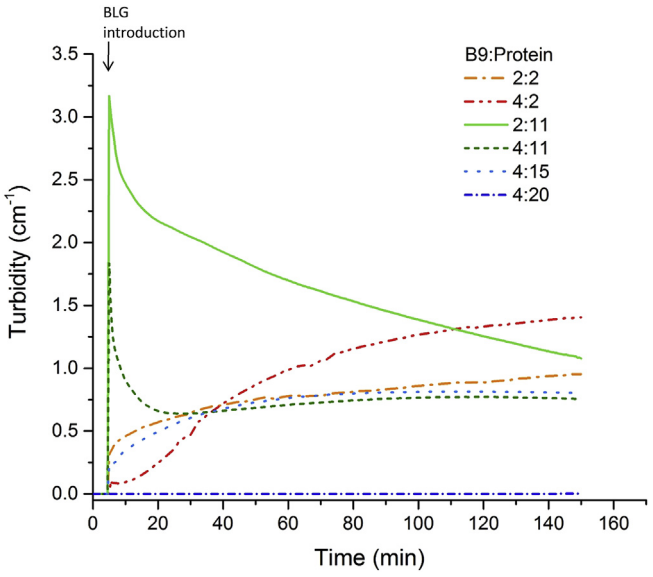

Fig. 1. Turbidity kinetics of LF-BLG co-assembly in the presence of B9 at six B9:protein mixing molar ratios spanning from low (0.1 mM) to high total protein concentration (1 mM), obtained at pH = 5.5 and at 20 °C. In this study, BLG/LF molar ratio of 10 was used.

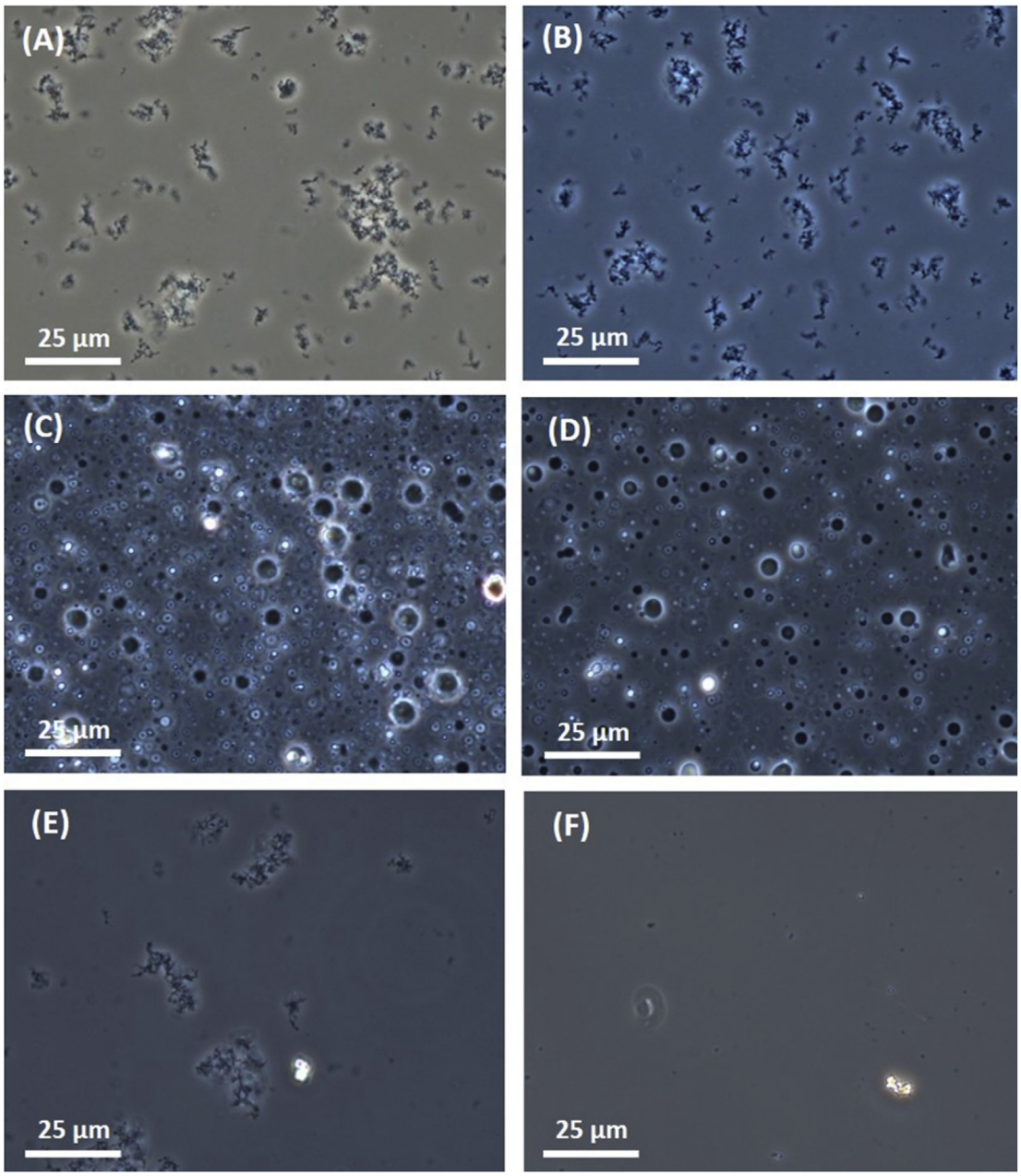

Fig. 2. Phase contrast microscopy (x40) of LF-BLG co-assembly in the presence of B9 at six B9:protein mixing molar ratios spanning from low (0.1 mM) to high total protein concentration (1 mM), obtained at pH = 5.5 and at 20 °C. (A) B9:protein = 2:2; (B) B9:protein = 4:2; (C) B9:protein = 2:11; (D) B9:protein = 4:11; (E) B9:protein = 4:15; (F) B9:protein = 4:20.

solutions with B9:protein ratios of low protein contents (2:2 and 4:2) and high protein content (4:15), exhibited a rather slow and gradual increase of turbidity toward a maximum asymptotic value (Fig. 1). These profiles corresponded to the formation of aggregates in the solutions (Fig. 2A, B, E). On the contrary, for the B9:protein ratios at intermediate protein contents (2:11 and 4:11), a sudden and high increase of turbidity was observed as soon as BLG was added followed by a slow and gradual decrease toward a minimum asymptotic value (Fig. 1). These profiles support a spontaneous process and corresponded to the formation of coacervates in the solutions (Fig. 2C, D). Finally, for the solution of very high protein content (4:20), no increased turbidity was observed (Fig. 1) and no supra-molecular structures were detected (Fig. 2F). Therefore, no significant co-assembly into large microparticles occurred between B9-LF-BLG at very high protein content.

These observations are consistent with literature on hetero-protein association. Moreover they are in adequacy with the previous results on BLG-LF co-assembly which have shown that BLG-LF aggregation occurred in solutions of low protein concentrations (Tavares, Croguennec, Hamon, et al., 2015). In addition (Yan et al., 2013), have mentioned that the formation of BLG-LF aggregates is a relatively slow and kinetically controlled process. Hence, it is likely that co-assembly by aggregation occurred in solutions with B9:protein ratios at low protein contents (2:2 and 4:2). Furthermore (Tavares, Croguennec, Hamon, et al., 2015), have reported that for intermediate protein content, the co-assembly between BLG and LF is spontaneous and lead to the formation of BLG-LF coacervates. It can therefore be supposed that complex coacervation occurred in the presence of B9 at intermediate protein contents (2:11 and 4:11). Moreover (Tavares, Croguennec, Hamon, et al.,

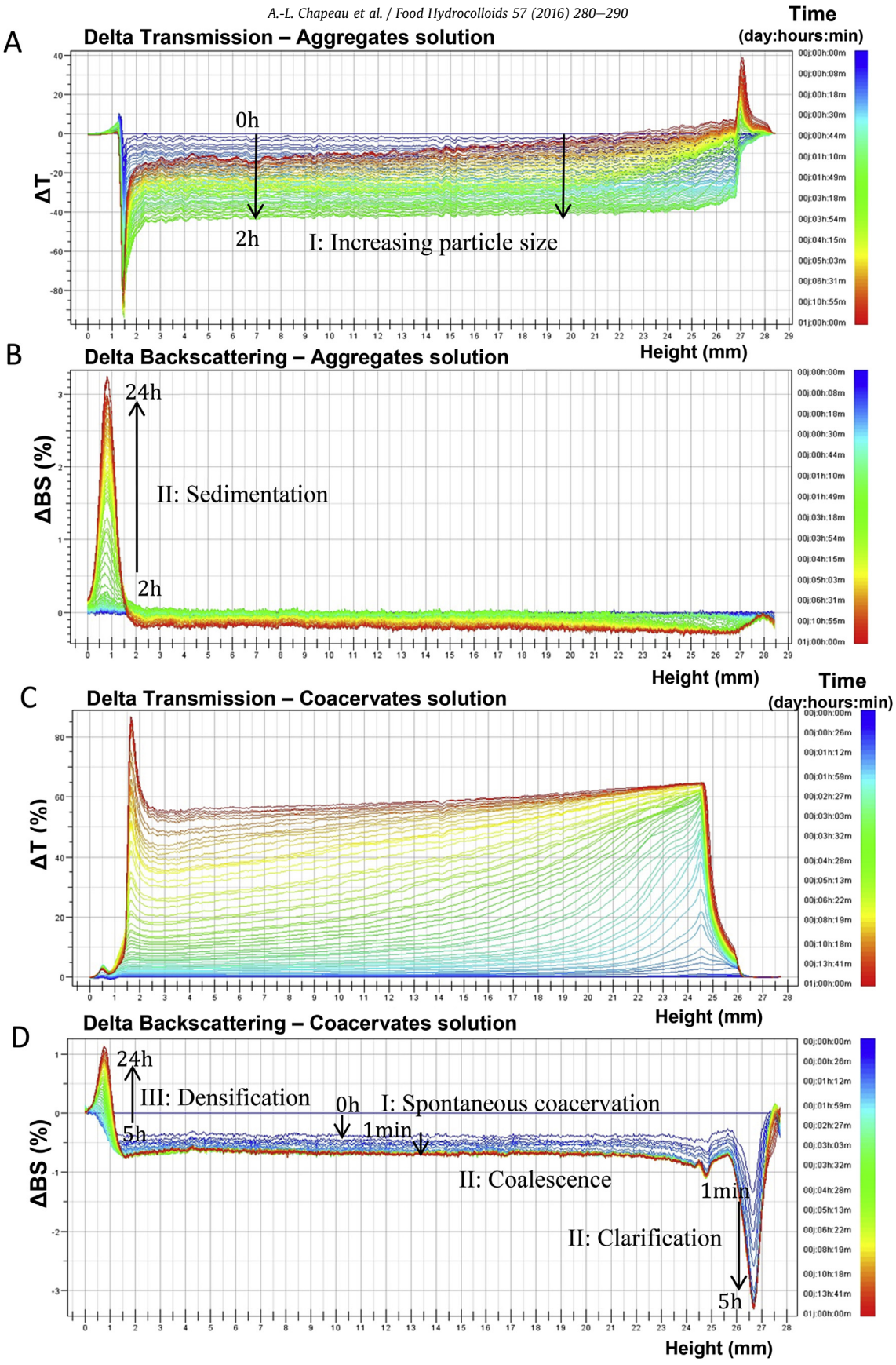

Fig. 3. Stability analysis of LF-BLG co-assemblies in the presence of B9 0.25 mM. Delta transmission and delta backscattering signals recorded over 24 h of formed aggregates (1.1 mM total proteins) (A, B) or coacervates (0.55 mM total proteins) (C, D) obtained at pH = 5.5 and at 20 °C. The backscattering intensity depends on particle size and concentration. It allowed to describe the evolution of the aggregate (B) or coacervate (D) particles as indicated by Roman numerals.

2015), have described that at high total protein concentrations, self-suppression of complex coacervation appears with a transition from coacervates to aggregates formation. This phenomenon can also be observed here for the solution with high protein content (4:15). Finally, an absence of supramolecular co-assembly into microparticles between BLG and LF has been previously reported for very high total protein concentrations by (Yan et al., 2013). Similarly, the absence of microparticles can be identified here for the solution of very high protein content (4:20). As a result, although FA interacts with LF under used experimental conditions forming small FA/LF nanoparticles (Tavares, Croguennec, Lê, et al., 2015), it does not prevent co-assembly between LF and BLG. Under these conditions, no interaction was detected between FA and BLG (not shown).

3.2. Stability of the co-assemblies

The stability of the two types of co-assembly (aggregates and coacervates) was evaluated in order to give insight into the evolution of the two types of co-assembly in solution, overtime. Stability of co-assembly solutions were assessed using optical characterization method with a TurbiScan. Two solutions were tested: one for the aggregates type of co-assembly (high concentration = 1.1 mM) and one for the coacervates type of co-assembly (intermediate protein concentration = 0.55 mM). In both solutions, B9 concentration was set at 0.25 mM. The first scan was realized immediately after mixing B9, LF and BLG solutions together and considered as the reference scan. Fig. 3 presents the patterns of delta transmission and delta backscattering obtained after subtraction of the reference scan.

For the solution of aggregates, delta transmission signal decreased progressively during the first 2 h, throughout the entire height of the tube (Fig. 3A). This indicated a gradual increase of the size of the aggregates in solution over the first 2 h. After 2 h, the delta backscattering signal started to increase between 0 and 2 mm height (Fig. 3B). This indicated a sedimentation of the aggregates at the bottom of the tube. For the solution of coacervates, delta backscattering signal showed an important drop over the first 1 min, indicating the spontaneous formation of supra-molecular structures (Fig. 3D). Then, the delta backscattering signal decreased between the 24–28 mm height of the tube (Fig. 3D), as well as an increase of the delta transmission signal (Fig. 3C). This phenomenon was important during 5 h and then remained relatively constant, demonstrating a rapid clarification at the top of the tube during the first 5 h. At the same time, the delta backscattering signal in the middle of the tube (2–24 mm height) was slightly decreasing (Fig. 3D). This indicated that the solution of coacervates became more opaque and thick over time. As the clarification at the top of tube happened at the same time, it can be deduced that the coacervates tended to coalesce together. From the fifth hour until 24 h, the delta backscattering signal of the coacervate solutions increased between 0 and 2 mm height (Fig. 3D), indicating a densification of the solution at the bottom of the tube.

These observations are in agreement with those presented on Figs.1 and 2, and give more insights into the kinetics of formation and the stability of the co-assemblies in solutions. In the case of aggregation (low and high protein contents), the formation of co-assembly seems to be a relatively slow process. Turbidity (Fig. 1) as well as the size of the particles or their number increased slowly over 2 h (Fig. 3A). Then, due to their density, aggregates tend to settle, creating a concentrated sediment phase (Fig. 3A). On the contrary, the formation of coacervates appears as a spontaneous co-assembly. Turbidity increased rapidly after BLG addition in the solutions of intermediate protein contents (2:11, 4:11) (Fig. 1) and particles around 10 μm can be observed just 5 min after the mixing of the three solutions (Fig. 2C), which correlates the observations made on Fig. 3D. The decrease of turbidity observed for the solutions of coacervates at intermediate protein contents (2:11 and 4:11) on Fig. 1 could be linked either to dissociation or coalescence and sedimentation of the coacervates. Fig. 3D shows that it is more likely that coacervate droplets coalesced together. This coalescence lead to the formation of larger coacervate droplets, which separated by gravity from the dilute phase. This dense phase formation is consistent with the literature on the theory of complex coacervation in protein systems. Some authors (de Kruif et al., 2004) and more recently (Bouhallab & Croguennec, 2014; Kizilay, Kayitmazer, & Dubin, 2011) reported that complex coacervation leads to the formation of a very concentrated phase of biopolymers. This results from the attractive interactions occurring between oppositely charged biopolymers in solution, which lead to phase separation and to the formation of a concentrated phase of coacervates. Furthermore (de Kruif et al., 2004) pointed out that these coacervates can be seen as a new colloidal entity. Thus, the coacervates formed here were obtained spontaneously by the electrostatic interactions occurring between positively charged LF and negatively charged BLG and B9 and their subsequent phase separation. As a result, the mixing of the three solutions lead overtime to the formation of a two phases system: the upper phase

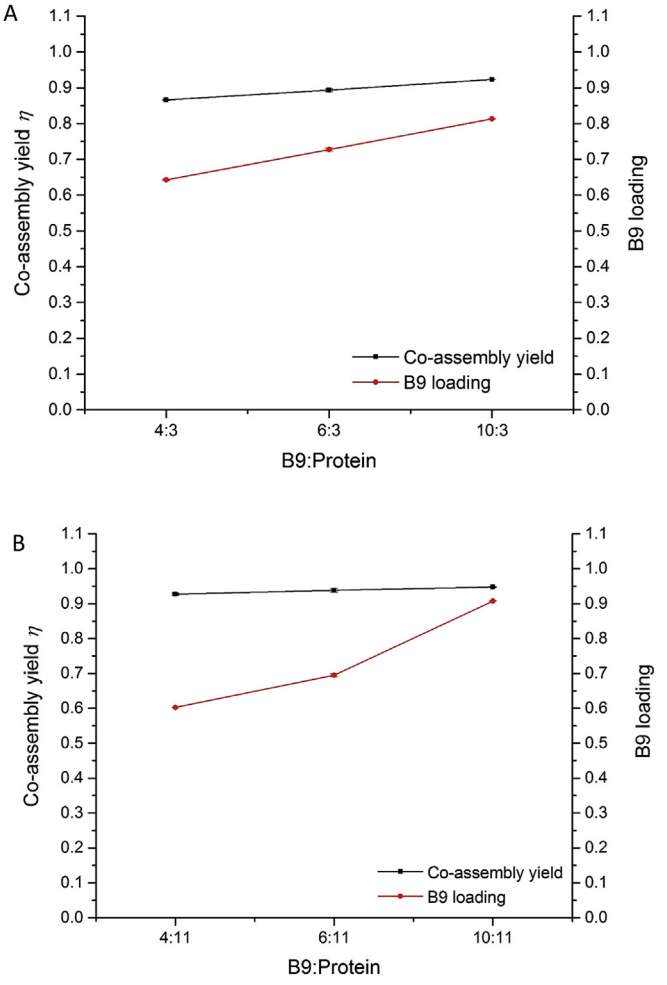

Fig. 4. Co-assembly yield η and B9 loading of B9-LF-BLG co-assembly at three different initial B9 contents and B9:protein mixing molar ratios at two total protein concentrations: (A) 0.15 mM and (B) (0.55 mM). Experiment were performed at pH = 5.5 and 20 °C.

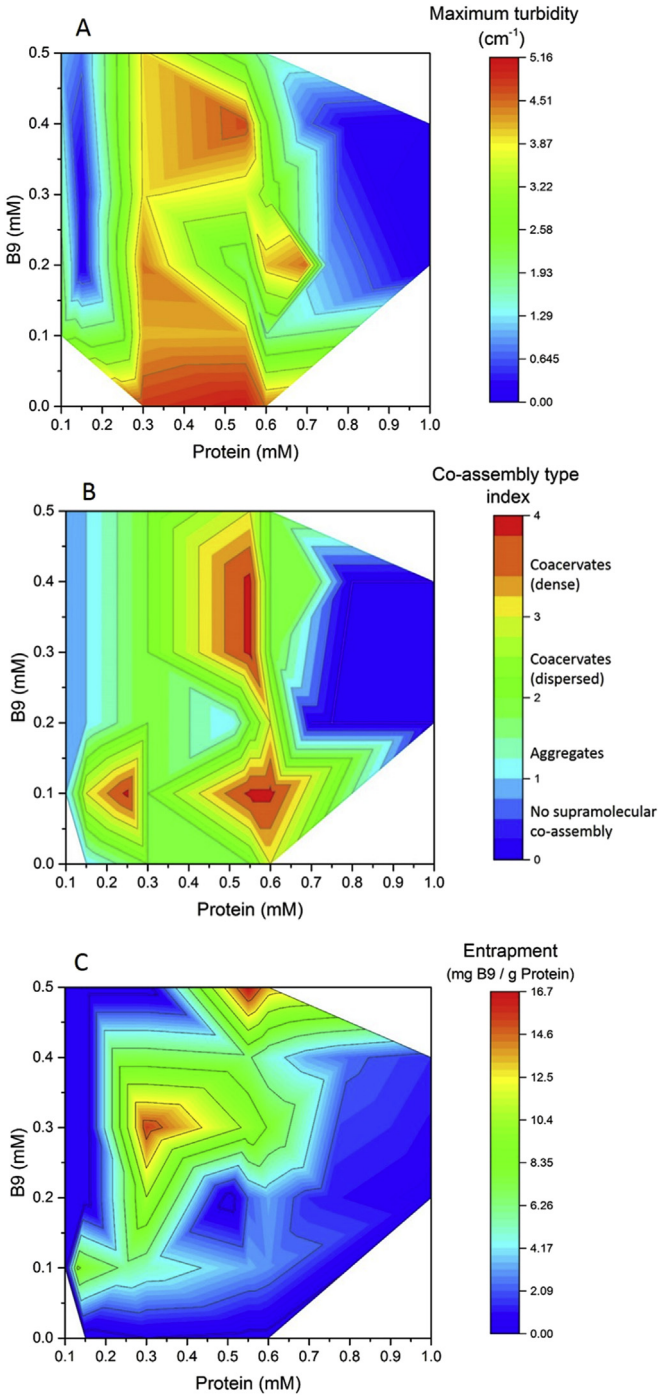

Fig. 5. Screening maps of B9-LF-BLG co-assembly by color projection for large range of B9 and protein concentrations at pH = 5.5 and at 20 °C. (A) maximum turbidity in cm^{-1}; (B) co-assembly type index; (C) entrapment in mg B9/g Protein.

was depleted of co-assemblies and the lower phase was concentrated in aggregates or coacervates, which possibly formed a biocarrier loaded with B9.

3.3. B9-LF-BLG co-assembly yield and B9 loading

To assess the co-assembly yield η of the two types of co-assembly, two protein contents were chosen: a low protein concentration, i.e. 0.11 mM for aggregates (Fig. 4A), and an intermediate protein concentration, i.e. 0.55 mM for coacervates (Fig. 4B). For both conditions, the BLG/LF molar ratio was constant and was equal to 10. At a set protein content, increased contents of B9 was tested to evaluate the B9 loading of each type of co-assembly.

For the two types of co-assembly, η increased as B9 increased (Fig. 4A and B). The solutions of B9-LF-BLG aggregates showed a co-assembly yield ranging from 0.85 to 0.90 (Fig. 4A). The solutions of B9-LF-BLG coacervates showed a co-assembly yield ranging from 0.90 to 0.95 (Fig. 4B). Thus, by comparing the two types of co-assembly, slightly higher co-assembly yields were obtained in the coacervation conditions. Correspondingly, B9 loading increased from 0.64 to 0.80 for aggregates solutions (Fig. 4A), and from 0.60 to 0.90 for coacervates solutions (Fig. 4B), as the content of B9 increased in the B9-LF-BLG solutions. The highest B9 loading obtained was 0.90 for a co-assembly yield of 0.95, obtained for the B9:protein ratio of 10:11. Thus, it can be assumed that the increase of the co-assembly yield is correlated with the increase of B9 in the solutions which leads to an increasing B9 loading throughout its entrapment within the B9-LF-BLG co-assembly. Optimal loading conditions were further sought by exploring a wider range of B9:protein ratios.

3.4. Screening maps of B9-LF-BLG co-assemblies

Screening maps were plotted in order to identify the domains of B9-LF-BLG co-assembly (maximum turbidity), their types (aggregates or coacervates) and the corresponding entrapment of B9. Fig. 5 presents the screening maps obtained by color projection of maximum turbidity (Fig. 5A), co-assembly type index (Fig. 5B) and the entrapment (Fig. 5C) as a function of the concentration of B9 and proteins.

It can be seen on Fig. 5A that no or little turbidity (dark blue color) was globally observed at low (0.1–0.2 mM) or high protein concentrations (0.7–0.85 mM). At intermediate protein concentrations (0.3–0.7 mM), the maximum turbidity increased (light green to red) and varied with B9 concentration. In this range of medium protein concentrations, these variations reveal two domains of maximum turbidity: the first one around 0.05 mM B9 the second one around 0.4 mM B9. In addition, rather similar observations can be drawn from the co-assembly type index (Fig. 5B). For low (0.1–0.2 mM) and high protein (0.7–0.85 mM) concentrations, no microparticles was observed which is consistent with the low maximum turbidity reached (Fig. 5A). The hydrodynamic diameters measured by DLS in these samples were found to be lower than 10 nm. Depending on the B9 and protein concentrations, three domains of maximum coacervation (yellow to red colors) can be evidenced: two at 0.1 mM B9 and protein concentrations of 0.25 and 0.6 mM and one at 0.35 mM B9 and protein concentration of 0.55 mM. These domains corresponded to the domains where co-assembly into coacervates were the densest. In the vicinity of these domains, the co-assembly type index decreased from 4 to 2, indicating less dense coacervation. Further, a transition toward co-assembly into aggregates was observed. These results corroborate those presented in Figs. 1 and 2. Furthermore, the two screening maps (Figs. 5A and B) appear to be rather similar, without being exactly identical. As a result, the compilation of these screening maps better evidenced the overall domains of no supramolecular co-assembly into microparticles, aggregation or coacervation, depending on B9 and protein concentrations and therefore on the B9:protein ratios. The domains of no microparticles co-assembly corresponded clearly to the solutions with protein concentration above 0.85 mM. B9-LF-BLG aggregates were favored at low (0.1–0.2 mM) and high protein concentrations (0.7–0.85 mM). Preferential domains of coacervation were found at intermediate

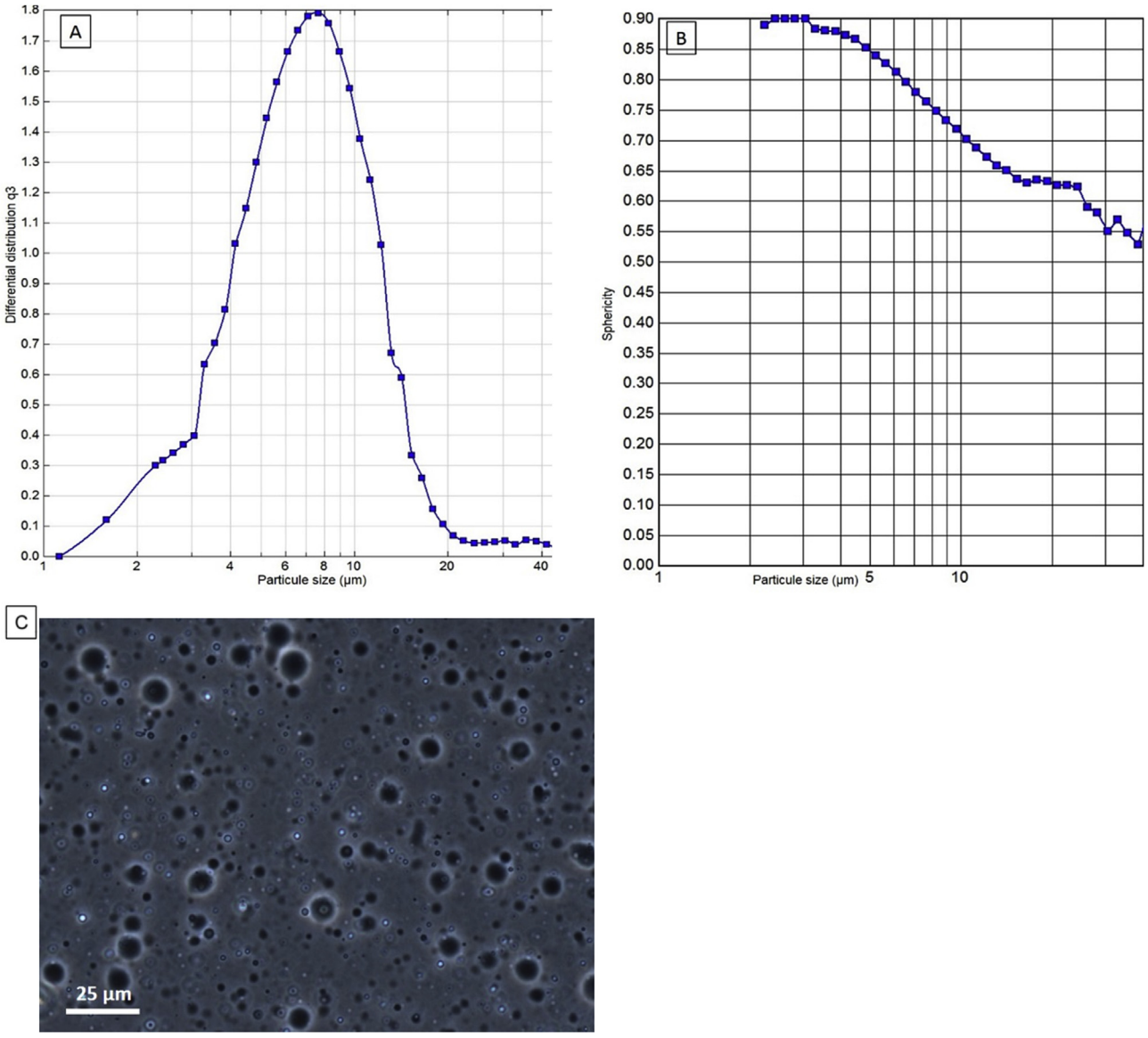

Fig. 6. Characteristics of B9-LF-BLG coacervates. (A) size distribution; (B) sphericity index; (C) image from phase contrast microscopy. Coacervates were obtained at B9 concentration of 0.25 mM and protein concentration of 0.55 mM), pH = 5.5 and at 20 °C.

protein concentrations between 0.3 and 0.7 mM with either low (0–0.1 mM) or intermediate (0.25–0.45 mM) B9 concentrations.

Two domains of high entrapment (red color) were identified (Fig. 5C): one at 0.3 mM B9 and protein concentration of 0.3 mM and one at 0.5 mM B9 and protein concentration of 0.6 mM (Fig. 5C), with an entrapment around 16.7 mg B9/g protein. In the vicinity of these domains, the entrapment decreased progressively from 16 to 8 mg B9/g protein. Above 0.7 mM of proteins, the entrapment kept on decreasing to low values from 6 mg B9/g protein (light blue color) to 0 mg B9/g protein (dark blue color). Hence, low B9 entrapment values were found for low (0.1–0.2 mM) and high protein concentration ranges (0.7–0.85 mM), both ranges where the formation of aggregates rather than coacervates was favored.

Compiling the three screening maps of Fig. 5 evidenced the entrapment of each type of co-assembly. The domains of no microparticles co-assembly and of aggregates formation identified at low and high protein concentrations appeared to be in the domains of lower entrapment for B9. On the contrary, the domains of high entrapment matched relatively well the domains of coacervation (co-assembly type index > 2 and maximum turbidity > 3 cm^{-1}) obtained for intermediate protein concentrations from 0.3 to 0.7 mM and for B9 concentrations from 0.1 to 0.4 mM.

These screening maps constitute a useful tool to predict the type of B9-LF-BLG co-assembly and the corresponding entrapment efficiency that can be obtained from the B9-LF-BLG co-assembly at different initial molar ratios. The compilation of these observations with the co-assembly type screening map evidences that the best B9 loading efficiencies are obtained for the B9:protein ratios of coacervates. The B9-LF-BLG coacervates obtained will lead to an entrapment ranging from 6 to 16 mg B9/g protein that corresponded to an entrapment efficiency ranging from 80 to 97% of B9.

Using nanospraydrying or electrospraying of whey protein concentrates as encapsulating technics, an entrapment of 12 mg B9/g total proteins has been recently reported (Pérez-Masiá et al., 2015). Therefore, the entrapment of B9 obtained here by spontaneous co-assembly is in the same range of order. Moreover (Diarrassouba, Remondetto, et al., 2015) have reported that the

coacervates obtained by the co-assembly between BLG and lysozyme for the design of vitamin D_3 biocarriers lead to a loading efficiency of ≈30 mg L^{-1} which corresponds to few μg per mg of proteins matrix as they prepared a solution at 0.1% of BLG. Moreover, the recommended daily intake for vitamin B9 is around 200–400 μg for adults and 400–800 μg for the vulnerable populations such as elderly or pregnant women. Thus, few milligrams of the B9-LF-BLG coacervates could cover the daily requirement for the vitamin. As a result, the spontaneous co-assembly of B9, LF and BLG into coacervates appeared as a viable and efficient process to design biocarriers for vitamin B9.

3.5. Characterization of B9-LF-BLG coacervates

Further analyses were performed on B9-LF-BLG coacervates obtained with 0.25 mM B9 and 0.55 mM total proteins. This composition of B9 and protein concentrations combined all at once provided a favorable co-assembly type index of 3, which corresponded to a quite dense coacervate formation (Fig. 5B), with a maximum turbidity of 3.5 cm^{-1} (Fig. 5A) and a good entrapment of 8 mg B9/g protein. Fig. 6 shows the volume size distribution and the sphericity index as a function of the particles size, for the coacervates obtained with the B9:protein ratio of 5:11. The size of the coacervates ranged from 2 to 20 μm diameter, with a mean diameter around 8 μm (Fig. 6A). The sphericity index of the coacervate droplets with 2–3 μm diameter was between 0.9 and 0.85 (Fig. 6B.). As the size of the coacervate droplets increased, sphericity index decreased. For coacervate droplets of 3–20 μm diameter, the sphericity index ranged from 0.85 to 0.60 (Fig. 6B). For coacervate droplets of 20 μm diameter and more, the sphericity index dropped to 0.50. Hence, small coacervates up to 5 μm diameter were almost perfect spherical droplets. For coacervates between 5 and 20 μm the sphericity was altered, suggesting less spherical droplets, e.g. formation of prolate type shape. A possible explanation for this result may be the coalescence that has been previously shown in coacervate solutions (Fig. 3D). The coalescence probably decreased the sphericity of the coacervates. The microscopic image on Fig. 6C obtained by phase contrast microscopy of the same B9:protein solution confirmed these observations. Thus, B9-LF-BLG coacervates are spherical droplets or slightly ovoid if they results from coalescence, with a mean diameter of 8 μm.

According to the experimental conditions, the B9-LF-BLG coacervate sizes were in the range of the BLG-LF coacervates sizes already reported: from 2.5 to 7.5 μm (Tavares, Croguennec, Hamon, et al., 2015) and 10–20 μm (Kizilay et al., 2014). Hence, the presence of B9 does not modify the overall size of BLG-LF coacervates. Furthermore (Diarrassouba, Remondetto, et al., 2015), have reported that the co-assembly between BLG and lysozyme for the design of biocarriers for vitamin D_3 led to the formation of spherical particles of 6–8 μm. This D_3-BLG-lysosyme co-assembly can be viewed as similar as the B9-LF-BLG coacervates formed here, although D_3 is a hydrophobic molecule while B9 is a hydrophilic one.

4. Conclusion

This work demonstrated that BLG and LF can form two types of microparticles, aggregates or coacervates, in the presence and absence of B9, showing that the presence of B9 does not interfere with the co-assembly between the two whey proteins. Moreover, B9-LF-BLG coacervates were formed spontaneously and showed a relative stability, prone to a slight coalescence overtime. On the contrary, B9-LF-BLG aggregation was a rather long and kinetically controlled process and aggregates were subject to significant sedimentation. B9-LF-BLG coacervates showed high entrapment of B9 which ranged from 6 to 16 mg B9/g protein. This entrapment rate is consistent with other technologies for the design of B9 biocarriers, and few mg of these coacervates can cover the recommended daily intake of B9. Consequently, we present a proof-of-concept study demonstrating that BLG-LF coacervates constitutes an efficient process to design biocarrier for vitamin B9. These results are promising to explore the potentialities of B9-LF-BLG coacervates for the development of natural and functional foods. Further studies should now be undertaken to assess the stability of these microparticles as biocarrier over time and during processing. Also, studies are required to shed light into whether these co-assemblies are able to protect B9 from photodegradation and oxidation and to assess the bioavailability of B9 loaded in such biocarriers.

Acknowledgment

We are grateful to Regional councils of Brittany (grant n° 13008651) and Pays de la Loire (grant n° 2014-07081) and INRA for the financial support of this work through the interregional project PROFIL, supported by BBA industrial association and managed by the “Pôle Agronomique Ouest”.

References

Adank, C., Green, T. J., Skeaff, C. M., & Briars, B. (2003). Weekly High-Dose folic acid supplementation is effective in lowering serum homocysteine concentrations in women. *Annals of Nutrition and Metabolism, 47*(2), 55–59. http://doi.org/10.1159/000069278.

Anema, S. G., & (Kees) de Kruif, C. G. (2014). Complex coacervates of lactotransferrin and β-lactoglobulin. *Journal of Colloid and Interface Science, 430*, 214–220. http://doi.org/10.1016/j.jcis.2014.05.036.

Annunziata, A., & Vecchio, R. (2011). Functional foods development in the European market: a consumer perspective. *Journal of Functional Foods, 3*(3), 223–228. http://doi.org/10.1016/j.jff.2011.03.011.

Araújo, M. M., Marchioni, E., Villavicencio, A. L. C. H., Zhao, M., di Pascoli, T., Kuntz, F., et al. (2015). Mechanism of folic acid radiolysis in aqueous solution. *LWT - Food Science and Technology, 63*(1), 599–603. http://doi.org/10.1016/j.lwt.2015.03.038.

Basset, G. J. C., Quinlivan, E. P., Gregory, J. F., & Hanson, A. D. (2005). Folate Synthesis and metabolism in plants and prospects for biofortification. *Crop Science, 45*(2), 449. http://doi.org/10.2135/cropsci2005.0449.

Betoret, E., Betoret, N., Vidal, D., & Fito, P. (2011). Functional foods development: trends and technologies. *Trends in Food Science & Technology, 22*(9), 498–508. http://doi.org/10.1016/j.tifs.2011.05.004.

Biesalski, H.-K., Dragsted, L. O., Elmadfa, I., Grossklaus, R., Müller, M., Schrenk, D., et al. (2009). Bioactive compounds: definition and assessment of activity. *Nutrition, 25*(11–12), 1202–1205. http://doi.org/10.1016/j.nut.2009.04.023.

Bouhallab, S., & Croguennec, T. (2014). Spontaneous assembly and induced aggregation of food proteins. In M. Müller (Ed.), *Polyelectrolyte complexes in the dispersed and solid state II* (pp. 67–101). Springer Berlin Heidelberg. Retrieved from http://link.springer.com/chapter/10.1007/12_2012_201.

Bungenberg de Jong, H.. (1949) (H.R. Kruit (Ed.)). London (1949).

Champagne, C. P., & Fustier, P. (2007). Microencapsulation for the improved delivery of bioactive compounds into foods. *Current Opinion in Biotechnology, 18*(2), 184–190. http://doi.org/10.1016/j.copbio.2007.03.001.

Chen, L. Y., Remondetto, G. E., & Subirade, M. (2006). Food protein-based materials as nutraceutical delivery systems. *Trends in Food Science & Technology, 17*(5), 272–283. http://doi.org/10.1016/j.tifs.2005.12.011.

Diarrassouba, F., Garrait, G., Remondetto, G., Alvarez, P., Beyssac, E., & Subirade, M. (2015). Food protein-based microspheres for increased uptake of vitamin D3. *Food Chemistry, 173*, 1066–1072. http://doi.org/10.1016/j.foodchem.2014.10.112.

Diarrassouba, F., Remondetto, G., Garrait, G., Alvarez, P., Beyssac, E., & Subirade, M. (2015). Self-assembly of β-lactoglobulin and egg white lysozyme as a potential carrier for nutraceuticals. *Food Chemistry, 173*, 203–209. http://doi.org/10.1016/j.foodchem.2014.10.009.

Diaz, J. (2013). How to clean up your label. *The World of Food Ingredients*. April/May, 10,12,14,16. Retrieved from http://repository.tudelft.nl/view/tno/uuid%3Ae64e9331-2e20-4caf-92e1-6d47b6be35f2/.

Eratte, D., Wang, B., Dowling, K., Barrow, C. J., & Adhikari, B. P. (2014). Complex coacervation with whey protein isolate and gum arabic for the microencapsulation of omega-3 rich tuna oil. *Food & Function, 5*(11), 2743–2750. http://doi.org/10.1039/c4fo00296b.

Ezhilarasi, P. N., Karthik, P., Chhanwal, N., & Anandharamakrishnan, C. (2013). Nanoencapsulation techniques for food bioactive components: a review. *Food and Bioprocess Technology, 6*(3), 628–647. http://doi.org/10.1007/s11947-012-0944-0.

Fang, Z., & Bhandari, B. (2010). Encapsulation of polyphenols - a review. *Trends in Food Science & Technology, 21*(10), 510–523.
Gouin, S. (2004). Microencapsulation: industrial appraisal of existing technologies and trends. *Trends in Food Science & Technology, 15*(7–8), 330–347. http://doi.org/10.1016/j.tifs.2003.10.005.
Gregory, J. F. (2001). Case study: folate bioavailability. *The Journal of Nutrition, 131*(4 Suppl), 1376S–1382S.
Hamilton, P., Littlejohn, D., Nordon, A., Sefcik, J., & Slavin, P. (2012). Validity of particle size analysis techniques for measurement of the attrition that occurs during vacuum agitated powder drying of needle-shaped particles. *The Analyst, 137*(1), 118–125. http://doi.org/10.1039/c1an15836h.
He, W., Parowatkin, M., Mailänder, V., Flechtner-Mors, M., Graf, R., Best, A., et al. (2015). Nanocarrier for oral peptide delivery produced by polyelectrolyte complexation in nanoconfinement. *Biomacromolecules, 16*(8), 2282–2287. http://doi.org/10.1021/acs.biomac.5b00500.
Hosseini, S. M. H., Emam-Djomeh, Z., Sabatino, P., & Van der Meeren, P. (2015). Nanocomplexes arising from protein-polysaccharide electrostatic interaction as a promising carrier for nutraceutical compounds. *Food Hydrocolloids, 50*, 16–26. http://doi.org/10.1016/j.foodhyd.2015.04.006.
Kizilay, E., Kayitmazer, A. B., & Dubin, P. L. (2011). Complexation and coacervation of polyelectrolytes with oppositely charged colloids. *Advances in Colloid and Interface Science, 167*(1–2), 24–37. http://doi.org/10.1016/j.cis.2011.06.006.
Kizilay, E., Seeman, D., Yan, Y., Du, X., Dubin, P. L., Donato-Capel, L., et al. (2014). Structure of bovine beta-lactoglobulin-lactoferrin coacervates. *Soft Matter, 10*(37), 7262–7268. http://doi.org/10.1039/c4sm01333f.
Kowalska, M., Zbikowska, A., & Tarnowska, K. (2015). Stability of emulsions containing interesterified fats based on mutton tallow and walnut oil. *Journal of the American Oil Chemists' Society, 92*(7), 993–1002. http://doi.org/10.1007/s11746-015-2659-7.
de Kruif, C. G., Weinbreck, F., & de Vries, R. (2004). Complex coacervation of proteins and anionic polysaccharides. *Current Opinion in Colloid & Interface Science, 9*(5), 340–349. http://doi.org/10.1016/j.cocis.2004.09.006.
Lacatusu, I., Mitrea, E., Badea, N., Stan, R., Oprea, O., & Meghea, A. (2013). Lipid nanoparticles based on omega-3 fatty acids as effective carriers for lutein delivery. Preparation and in vitro characterization studies. *Journal of Functional Foods, 5*(3), 1260–1269. http://doi.org/10.1016/j.jff.2013.04.010.
Liang, L., Leung Sok Line, V., Remondetto, G. E., & Subirade, M. (2010). In vitro release of α-tocopherol from emulsion-loaded β-lactoglobulin gels. *International Dairy Journal, 20*(3), 176–181. http://doi.org/10.1016/j.idairyj.2009.09.008.
Liang, L., Tremblay-Hébert, V., & Subirade, M. (2011). Characterisation of the β-lactoglobulin/α-tocopherol complex and its impact on α-tocopherol stability. *Food Chemistry, 126*(3), 821–826. http://doi.org/10.1016/j.foodchem.2010.12.029.
Lucock, M. (2000). Folic acid: nutritional biochemistry, molecular biology, and role in disease processes. *Molecular Genetics and Metabolism, 71*(1–2), 121–138. http://doi.org/10.1006/mgme.2000.3027.
Matalanis, A., Jones, O. G., & McClements, D. J. (2011). Structured biopolymer-based delivery systems for encapsulation, protection, and release of lipophilic compounds. *Food Hydrocolloids, 25*(8), 1865–1880. http://doi.org/10.1016/j.foodhyd.2011.04.014.
McClements, D. J. (2015). Encapsulation, protection, and release of hydrophilic active components: potential and limitations of colloidal delivery systems. *Advances in Colloid and Interface Science, 219*, 27–53. http://doi.org/10.1016/j.cis.2015.02.002.
McClements, D. J., Decker, E. A., & Park, Y. (2009). Controlling lipid bioavailability through physicochemical and structural approaches. *Critical Reviews in Food Science and Nutrition, 49*(1), 48–67. http://doi.org/10.1080/10408390701764245.
Mills, J. L., & Signore, C. (2004). Neural tube defect rates before and after food fortification with folic acid. *Birth Defects Research Part A: Clinical and Molecular Teratology, 70*(11), 844–845. http://doi.org/10.1002/bdra.20075.
Moat, S. J., Lang, D., McDowell, I. F. W., Clarke, Z. L., Madhavan, A. K., Lewis, M. J., et al. (2004). Folate, homocysteine, endothelial function and cardiovascular disease. *The Journal of Nutritional Biochemistry, 15*(2), 64–79. http://doi.org/10.1016/j.jnutbio.2003.08.010.
Overbeek, J. T. G., & Voorn, M. J. (1957). Phase separation in polyelectrolyte solutions. Theory of complex coacervation. *Journal of Cellular and Comparative Physiology, 49*(S1), 7–26. http://doi.org/10.1002/jcp.1030490404.
Pérez-Masiá, R., López-Nicolás, R., Periago, M. J., Ros, G., Lagaron, J. M., & López-Rubio, A. (2015). Encapsulation of folic acid in food hydrocolloids through nanospray drying and electrospraying for nutraceutical applications. *Food Chemistry, 168*, 124–133. http://doi.org/10.1016/j.foodchem.2014.07.051.
Ron, N., Zimet, P., Bargarum, J., & Livney, Y. D. (2010). Beta-lactoglobulin–polysaccharide complexes as nanovehicles for hydrophobic nutraceuticals in non-fat foods and clear beverages. *International Dairy Journal, 20*(10), 686–693. http://doi.org/10.1016/j.idairyj.2010.04.001.
Sanjoaquin, M. A., Allen, N., Couto, E., Roddam, A. W., & Key, T. J. (2005). Folate intake and colorectal cancer risk: a meta-analytical approach. *International Journal of Cancer, 113*(5), 825–828. http://doi.org/10.1002/ijc.20648.
Schmitt, C., Aberkane, L., & Sanchez, C. (2009). 16-Protein—polysaccharide complexes and coacervates. In G. O. Phillips, & P. A. Williams (Eds.), *Handbook of hydrocolloids* (2nd ed., pp. 420–476). Woodhead Publishing. Retrieved from http://www.sciencedirect.com/science/article/pii/B9781845694142500163.
Schmitt, C., Sanchez, C., Desobry-Banon, S., & Hardy, J. (1998). Structure and technofunctional properties of protein-polysaccharide complexes: a review. *Critical Reviews in Food Science and Nutrition, 38*(8), 689–753. http://doi.org/10.1080/10408699891274354.
Schmitt, C., & Turgeon, S. L. (2011). Protein/polysaccharide complexes and coacervates in food systems. *Advances in Colloid and Interface Science, 167*(1–2), 63–70. http://doi.org/10.1016/j.cis.2010.10.001.
Shimoni, E. (2009). Nanotechnology for foods: delivery systems by. In by, G. Barbosa-Canovas, A. Mortimer, D. Lineback, W. Spiess, K. Buckle, & P. Colonna (Eds.), *Global issues in food science and technology* (pp. 411–424). San Diego: Academic Press. Retrieved fromhttp://www.sciencedirect.com/science/article/pii/B9780123741240000235.
Tavares, G. M., Croguennec, T., Carvalho, A. F., & Bouhallab, S. (2014). Milk proteins as encapsulation devices and delivery vehicles: applications and trends. *Trends in Food Science & Technology, 37*(1), 5–20. http://doi.org/10.1016/j.tifs.2014.02.008.
Tavares, G. M., Croguennec, T., Hamon, P., Carvalho, A. F., & Bouhallab, S. (2015). Selective coacervation between lactoferrin and the two isoforms of beta-lactoglobulin. *Food Hydrocolloids, 48*, 238–247. http://doi.org/10.1016/j.foodhyd.2015.02.027.
Tavares, G. M., Croguennec, T., Lê, S., Lerideau, O., Hamon, P., Carvalho, A. F., et al. (2015). Binding of folic acid induces specific self-aggregation of lactoferrin: thermodynamic characterization. *Langmuir: The ACS Journal of Surfaces and Colloids, 31*(45), 12481–12488. http://doi.org/10.1021/acs.langmuir.5b02299.
Teng, Z., Li, Y., & Wang, Q. (2014). Insight into curcumin-loaded β-lactoglobulin nanoparticles: incorporation, particle disintegration, and releasing profiles. *Journal of Agricultural and Food Chemistry, 62*(35), 8837–8847. http://doi.org/10.1021/jf503199g.
de Vos, P., Faas, M. M., Spasojevic, M., & Sikkema, J. (2010). Encapsulation for preservation of functionality and targeted delivery of bioactive food components. *International Dairy Journal, 20*(4), 292–302. http://doi.org/10.1016/j.idairyj.2009.11.008.
Xiao, Z., Liu, W., Zhu, G., Zhou, R., & Niu, Y. (2014). A review of the preparation and application of flavour and essential oils microcapsules based on complex coacervation technology. *Journal of the Science of Food and Agriculture, 94*(8), 1482–1494.
Yan, Y., Kizilay, E., Seeman, D., Flanagan, S., Dubin, P. L., Bovetto, L., et al. (2013). Heteroprotein complex coacervation: bovine β-lactoglobulin and lactoferrin. *Langmuir, 29*(50), 15614–15623. http://doi.org/10.1021/la4027464.
Zhang, J., Liu, X., Subirade, M., Zhou, P., & Liang, L. (2014). A study of multi-ligand beta-lactoglobulin complex formation. *Food Chemistry, 165*, 256–261. http://doi.org/10.1016/j.foodchem.2014.05.109.